JGR Space Physics

RESEARCH ARTICLE
10.1029/2022JA030577

Applying Magnetic Curvature to MMS Data to Identify Thin Current Sheets Relative to Tail Reconnection

A. J. Rogers[1,2], C. J. Farrugia[1], R. B. Torbert[1], and T. J. Rogers[3]

[1]Space Science Center, University of New Hampshire, Durham, NH, USA, [2]Los Alamos National Laboratory, Los Alamos, NM, USA, [3]Microsoft Corporation, Redmond, WA, USA

Key Points:

- Distribution of ion-scale tail current sheets (CS) seen by MMS during 2017–2020 using magnetic curvature as proxy for CS thickness
- Location of tail CS with thickness at or below ion gyro-scale compared to location of reconnection-related Ion Diffusion Regions
- Observations compared to recent particle-in-cell simulations

Supporting Information:

Supporting Information may be found in the online version of this article.

Correspondence to:

A. J. Rogers,
arogers@lanl.gov

Citation:

Rogers, A. J., Farrugia, C. J., Torbert, R. B., & Rogers, T. J. (2023). Applying magnetic curvature to MMS data to identify thin current sheets relative to tail reconnection. *Journal of Geophysical Research: Space Physics*, *128*, e2022JA030577. https://doi.org/10.1029/2022JA030577

Received 26 JUL 2022
Accepted 30 DEC 2022

Author Contributions:

Funding acquisition: R. B. Torbert
Resources: C. J. Farrugia
Software: T. J. Rogers
Supervision: C. J. Farrugia, R. B. Torbert
Writing – review & editing: C. J. Farrugia

Abstract Thin current sheets (TCSs) have been postulated to be a necessary precondition for reconnection onset. Magnetic reconnection X-lines in the magnetotail have been observed to be more common duskward of midnight. We take advantage of the MMS tetrahedral formation during the 2017–2020 MMS tail seasons to calculate the thickness of the cross-tail neutral sheet relative to ion gyroradius. While a similar technique was applied to Cluster data, current sheet thickness over a broader range of radial distances has not been robustly explored before this study. We compare our analysis to recent theories regarding mechanisms of tail current sheet thinning and to recent simulations. We find MMS spent more than twice as long in ion-scale TCSs in the pre-midnight sector than post-midnight, despite nearly even plasma sheet dwell time. The dawn-dusk asymmetry in the distribution of Ion Diffusion Regions, as previously reported in relation to regions of TCSs, is also analyzed.

Plain Language Summary Magnetic reconnection is an important mechanism for energy transfer in the magnetosphere. In order for reconnection to begin, however, the reconnecting current sheet must first become very thin. Reconnection and related phenomena have been observed in the geomagnetic tail closer to dusk than dawn on the nightside, although the reasons for this have not been clearly understood. Recent simulations of the geomagnetic tail suggest that the central current sheet in the tail should be thinner pre-midnight than post-midnight, possibly explaining why reconnection happens more often on the pre-midnight than the post-midnight sector. We use 19 months of MMS data in the tail, comprising the tail seasons of 4 years from 2017 to 2020, to estimate the thickness of the tail neutral sheet relative to relevant ion scales from dawn flank to dusk flank and both closer to and further away from the Earth than has been done in the past. We then compare the thickness we measure with the simulation predictions and with the location of previously identified reconnection locations in the same time period.

1. Introduction

In Dungey's model of the open magnetosphere (Dungey, 1961, 1963), magnetic field energy stored in the interplanetary magnetic field (IMF) is transferred to kinetic energy of the magnetospheric plasma in a process called magnetic reconnection. On the dayside, reconnection is between the IMF and that of the closed terrestrial magnetospheric field lines. In the tail, where the flux transported from the dayside loads and thins the tail current sheet (CS, embedded in the plasma sheet), reconnection closes the open flux and returns it to the dayside, leading to a two-cell plasma convection in the magnetosphere (see review by Cowley (1981)). This model has received abundant observational support.

Phenomena associated with reconnection in the geomagnetic tail such as auroral substorms, dipolarization fronts, and bursty-bulk flows as well as in situ observations of reconnection in the tail have provided an important part of this support. However, the locations of these phenomena have also shown a significant asymmetry in the dawn-dusk direction, being more common on the dusk-side of midnight by significant ratios (Y.-H. Liu et al., 2014; Nagai et al., 1998; Posch et al., 2007; Xiao et al., 2017). A statistical study using THEMIS (Sibeck & Angelopoulos, 2008) was performed by Imber et al. (2011) and showed that 81% of flux ropes and traveling compression regions associated with reconnection in the magnetotail were found in the dusk sector. A. J. Rogers et al. (2019) showed that reconnection regions (ion diffusion regions or IDRs) during the 2017 MMS tail season (May–September) were preferentially observed in situ on the dusk-side of midnight by a far larger ratio (91.7% pre-midnight, 8.3% post-midnight) than could be accounted for by differences in spacecraft dwell time on either side of midnight (56.5% pre-midnight, 43.5% post-midnight). This strongly suggests that the observed

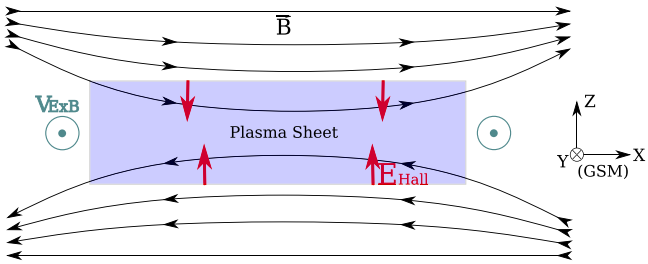

Figure 1. A schematic of a section of tail current sheet with thickness of ion-scale aligned with GSM coordinates. Heavy and super-thermal ions may demagnetize even when the bulk of the plasma population remains frozen-in. Once demagnetized, they will cause a weak Hall electric field due to charge separation from the electron population (red arrows). The $\vec{E} \times \vec{B}$ drift will accelerate the demagnetized particles (and the bulk plasma to a lesser extent) in the $-\hat{y}$ direction (i.e., dawnward, sea-green).

asymmetrical distribution of reconnection and related phenomena is due to underlying physical processes and not observational bias.

The common thread throughout all theories of magnetic reconnection is an initial condition of a thin current sheet (TCS) separating opposing magnetic fields. Various simulations have suggested the maximum current sheet thickness which would support reconnection onset is between several ion inertial lengths (Birn, 1980) and two electron inertial lengths (D. Liu et al., 2020) depending on the exact instability which instigates reconnection onset. Despite the continuing debate over the precise onset mechanism, it would seem that a central current sheet of thickness in the range of the ion gyroradius or smaller is a necessary precondition for magnetic reconnection in the tail. Thus, the distribution of ion-scale CS within the central tail plasma sheet is pertinent to the question of reconnection location in the tail by way of identifying where reconnection onset is even possible.

Attempts to estimate the thickness of the tail current sheet have occasionally been made using single-spacecraft measurement techniques (e.g., Artemyev et al., 2011; Lu et al., 2019; Sergeev et al., 1998). Many of these techniques relied on a ratio of measurements of the magnetic field and particle current density; often with a significant time separation between these two measurements. This assumes that the current sheet being measured is essentially a stationary current slab, similar to a Harris-type current sheet (Harris, 1962), that is, an infinitely long current sheet with uniform thickness and geometry, throughout the measurement period. However, reconnection and related substorm phenomena often occur during times of a disturbed geomagnetic field, limiting the utility of the Harris current sheet assumption.

There is a considerable body of work addressing the formation of TCSs in the magnetotail and how their thickness is estimated. Varied estimates of current sheet thickness using four-point magnetic field measurements have been made using Cluster (Asano et al., 2005; Nakamura et al., 2002; Petrukovich et al., 2007; Runov, Sergeev, Baumjohann, et al., 2005; Runov, Sergeev, Nakamura, et al., 2005). Rong et al. (2011), in particular, utilized the four spacecraft of the Cluster mission in tetrahedral formation to calculate the radius of curvature (R_C) of the magnetic field at the barycenter of the fleet:

$$R_C = \frac{1}{|(\hat{b} \cdot \nabla)\hat{b}|} \tag{1}$$

where $\hat{b}$ is the unit vector $\vec{B}/|\vec{B}|$. They then estimated the half-thickness of the neutral sheet by scaling the radius of curvature by the current sheet tilt angle θ such that $h = R_C \cos(\theta)$ where $\theta \approx \arctan(B_y/B_z)$, implying that $2R_C$ measured within the plasma sheet is a maximum estimate for the thickness of the neutral sheet (Rong et al., 2010, 2011; Shen et al., 2008). This method was superior to previous estimates using single-spacecraft techniques. A statistically significant dawn-dusk asymmetry in CS thinner than 1,000 km ($\sim$ an ion gyroradius in the tail plasma sheet) was found, with thinner CS more common duskward of midnight. However, due to the nature of its near-polar orbit, Cluster only sampled the current sheet at a radial distance of approximately 19 Earth Radii (R_E) from the Earth, although broadly in MLT. The physics of the near-Earth TCS formation was studied with 3-point THEMIS observations in a series of works by Artemyev, Angelopoulos, and Runov (2016), Artemyev, Angelopoulos, Runov, and Petrokovich (2016), and Artemyev et al. (2017); and Runov et al. (2021) have recently produced a comprehensive review of near-Earth current sheet thinning studies. Current sheet thickness in the geomagnetic tail has not been explored using techniques as robust as those employed by Rong et al. at other radial distances before this work.

The mechanism for current sheet thinning has also been explored in recent simulations. Hybrid and particle-in-cell (PIC) simulations (Lu et al., 2016, 2018) suggest that external drivers cause a global compression of the tail current sheet to approximately ion scales, at which point partial demagnetization of ions drives charge separation from the still frozen-in electrons, leading to Hall electric fields, although not necessarily reconnection. These demagnetized particles then move dawnward under $\vec{E} \times \vec{B}$ drifting (see Figure 1), partially evacuating ions from the duskside and leading to even greater dawnward flow under diamagnetic drift. This has the effect of progressive thinning of the pre-midnight current sheet toward the dusk flank. These simulations suggest the asymmetric thinning should be robust across a broad range of radial distances.

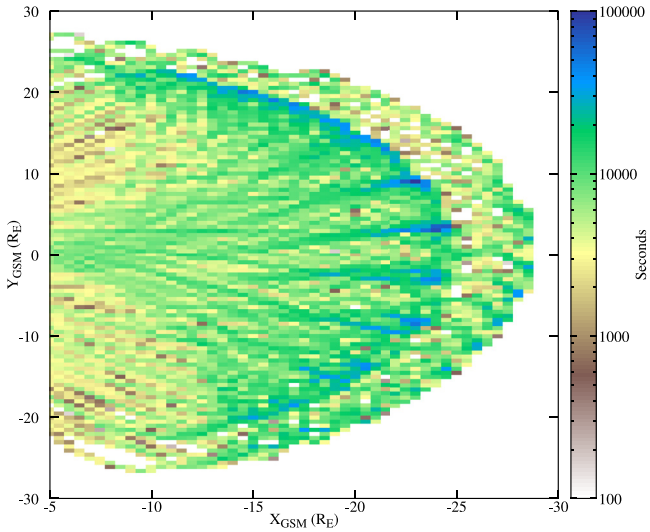

Figure 2. Plasma Sheet Dwell Time: The time in seconds (shown by colorbar scale) MMS spent within the tail plasma sheet as determined by plasma number density $n > 0.05$ *cc* during the 2017–2020 tail seasons.

We choose the instantaneous gyroradius at mean thermal energy of the local ion population, calculated using the average magnetic field magnitude across the four MMS observatories, as the test scale length to compare to the local current sheet thickness estimate to identify CS which may be preferentially thinned as suggested by simulations. This choice of scale length has theoretical support. Büchner and Zelenyi (1987, 1989) describe a mechanism for demagnetizing charged particles near a strong gradient in the magnetic field by testing violations of the first adiabatic invariant. They offer the ratio of minimum magnetic field line curvature radius to particle gyroradius as a scalar indicator of non-adiabatic motion of particles, and thus an indicator of demagnetization of charged particles. Applying this ratio K to ions:

$$K_i = \sqrt{\frac{R_C}{\rho_{g,i}}} \tag{2}$$

where $\rho_{g,i} = \frac{\sqrt{2m_i T_{\perp,i} k_b}}{q_i |\vec{B}|}$ is the thermal ion gyroradius. Where $K_i < 1$ the gyroradius of the thermal average ion is larger than the radius of curvature of the local magnetic field, implying that the majority of ions will encounter multiple guiding centers during a single gyroperiod, incompatible with ideal adiabatic motion. The degree of chaotic motion increases with decreasing values of K until ions become functionally demagnetized for values of $K_i < 0.2$ (Büchner & Zelenyi, 1989). Any degree of non-adiabatic motion ($K_i < 3$) will lead to charge separation and the formation of Hall electric fields, supporting the process described by Lu et al.

The same $K_i < 1$ condition, indicating that the thermal mean gyroradius is smaller than the half-thickness of the tail current sheet, is also indicative of a reasonable maximum current sheet thickness that might support magnetic reconnection. Therefore a map of the geomagnetic tail indicating regions where $K_i < 1$ will show what regions are most likely to support reconnection. Using data from the 2017–2020 MMS tail seasons and leveraging the regular tetrahedral formation of MMS along with the high-resolution magnetometers on board, the radius of curvature of magnetic field lines can be calculated and compared to the ion thermal gyroradius to calculate K_i throughout the tail central plasma sheet (see Figure 2).

The goal of this work is to examine the distribution of TCSs in the geomagnetic tail, in particular their dawn-dusk distribution. We target four MMS tail seasons, 2017–2020 (≈550 days). We adopt an approach based on the magnetic field line curvature. Thus, by "TCS" we mean here less than the ion gyroradius (typically $\approx 100 - 1{,}000$ km). This is obtained via the curvature-related parameter, K. We find and discuss the "observational bias" during these observations. The inter-spacecraft separation of the MMS observatories was typically ≈20 km, much less than in previous studies using the Cluster and Themis constellations. Since TCSs, as defined here, would favor magnetic reconnection, we then compare the resulting dawn-dusk distribution of TCSs with that of IDRs, which were identified in a previous study (A. J. Rogers et al., 2019). While dawn-dusk asymmetries in tail parameters and behavior have been discussed before using mainly Cluster and Themis observations, with typically larger inter-spacecraft separations (e.g., Runov et al., 2021; Sitnov et al., 2019), we believe that our work constitutes a valuable addition to these efforts.

2. Methodology and Software

The MMS spacecraft measure electric and magnetic fields using the FIELDS instrument suite (Torbert et al., 2016). The analog and digital fluxgate magnetometers (AFG/DFG) measure magnetic fields in the frequency range from DC up to 64 Hz (Russell et al., 2016). Level 2 fluxgate magnetometer (FGM) data of version 5.86 and higher (highest available as of submission) were used throughout this study.

The Fast Plasma Instrument (FPI) provides MMS with high cadence electron and ion distributions in the energy/charge range of 10 eV/q up to 30 keV/q. Each MMS satellite is equipped with eight FPI spectrometers which, combined with electrostatic control of the field-of-view, allows FPI to sample the full electron and ion distributions (Pollock et al., 2016). It is important to note that core ion distributions can extend beyond the range of

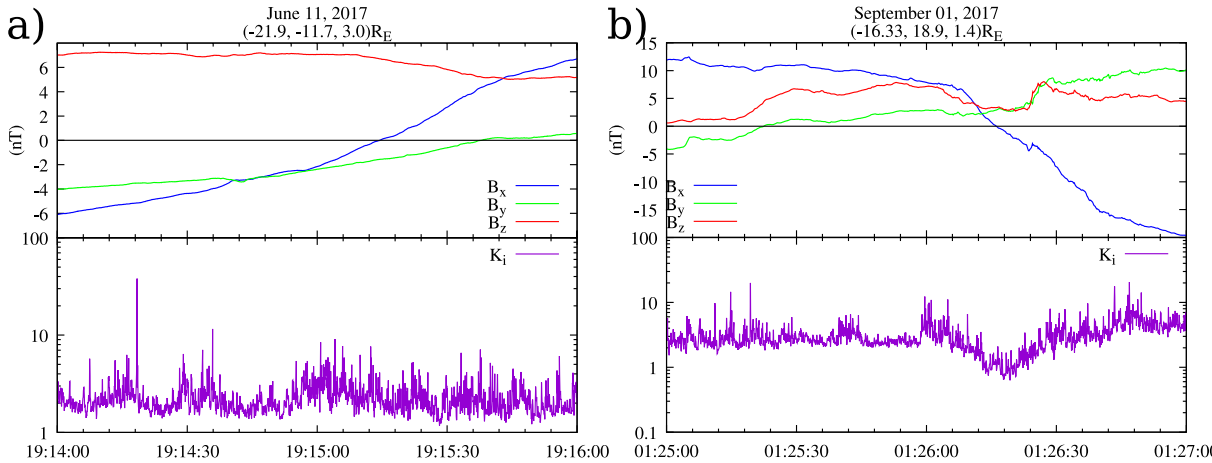

Figure 3. Two example central current sheet crossings made by MMS. Upper panels show the vector magnetic field in GSM coordinates. The lower panels show the values for K_i during each event on a log scale. All times are in UTC; positions of MMS during each event are given above in GSM coordinates. (a) A quiet current sheet (CS) encounter post-midnight. Note that K_i is never less than 1. (b) A CS encounter near the dusk flank. Note that $K_i < 1$ for approximately 5 s near 01:26:17 UTC.

FPI, meaning that actual ion temperatures may be higher than what is calculated using FPI data. Level 2 FPI ion moments of version 3.3.0 were used throughout this study.

Positions of the individual spacecraft in the MMS fleet are provided using Magnetic Ephemeris and Coordinates data products (Morley, 2015) and are calculated using the LANLGeoMag suite (Henderson et al., 2018). All instrument data used in this study is available from the MMS Science Data Center (https://lasp.colorado.edu/mms/sdc). Level 2 fast survey data was used throughout this study. Calculations of the magnetic field line curvature were made using the `mms-curvature` library and is publicly available (Rogers & Rogers, 2022).

In order to ensure that the formation of the MMS fleet was appropriate for the calculation of spatial gradients a minimum value of the Tetrahedron Quality Factor (TQF) (Fuselier et al., 2016) was required where $TQF \geq 0.8$. For similar reasons, this survey was performed only on data collected while the MMS fleet was at least eight Earth radii (R_E) from the Earth to avoid deformations of the regular tetrahedron as the fleet approached perigee. Observations in this study were also limited to regions with a measured ion density of $\rho_i \geq 0.05\ cc^{-1}$ to ensure they were made in the plasma sheet (Baumjohann, 1993; Raj et al., 2002; A. J. Rogers et al., 2019).

The high-resolution plasma (FPI) and magnetic field (FGM) instruments on board MMS (Pollock et al., 2016; Russell et al., 2016) allow for the calculation of K at high time cadence. The ion thermal gyroradius $\rho_{g,i}$ is easily calculated using the mean values of $T_\perp$ and $|\vec{B}|$ across all four spacecraft of the MMS fleet. The calculation of R_C is less straightforward and was accomplished using the `mms-curvature` python library (A. Rogers & Rogers, 2022). Analysis was completed using automated scripts written in python, examples of which are included with the `mms-curvature` library.

3. Observations and Analysis

Two example central tail current sheet encounters are shown in Figure 3. The half-thickness of the central neutral sheet is frequently greater than an ion gyroradius, indicated by a K_i value greater than one as shown in Figure 3a. More active central CS (characterized by greater $d|\vec{B}|/dt$ observed by MMS while traversing the central plasma sheet), such as that shown in Figure 3b, tend to have half-thicknesses equal to or less-than an ion gyroradius, as indicated by K_i values less than one. As more active central CS are also often characterized by significant motion of the neutral sheet (i.e., tail flapping and twisting) MMS encounters with such thin neutral sheets are often transient and each CS encounter may yield only a few second of measurements showing $K_i < 1$. As such, a statistical aggregation of such events may provide greater insight.

Figure 4 shows the distribution of ion-scale TCSs as measured by MMS over the combined 2017–2020 tail seasons where data from all four MMS spacecraft were available (≈550 days of data). Colors represent the amount of time which MMS spent in each region with a value of $K_i < 1.0$, that is, the dwell time of MMS

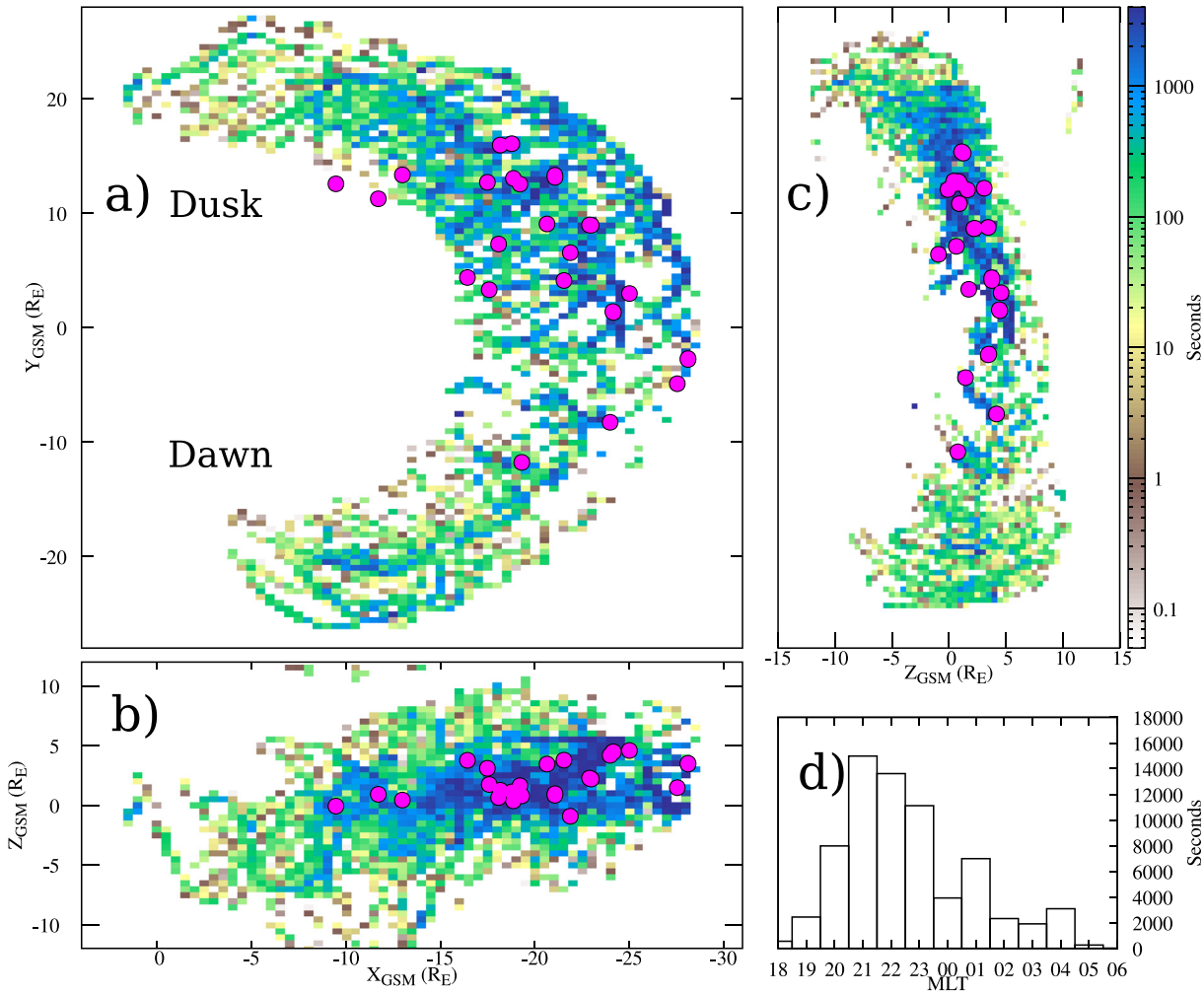

Figure 4. The total amount of time in seconds spent by MMS in a thin current sheet (TCS), under conditions outlined in the text, in sectors of dimension $0.5R_E \times 0.5R_E$ (a–c) and Magnetic Local Time (MLT) (d). (a) Distribution of TCS dwell times in the GSM *X*–*Y* plane, with times summed over the GSM *Z* axis. (b) TCS dwell times in the GSM *X*–*Z* plane, with times summed over the GSM *Y* axis. (c) TCS dwell times in the GSM *Z*–*Y* plane, with times summed over the GSM *X* axis. (d) TCS dwell times across all radial distances by MLT location. Magenta circles represent Ion Diffusion Region locations (see text).

in a current sheet thinner than an ion gyroradius at the time. The effects of orbital or observational bias on these dwell time measurements are small as MMS spent approximately equal time in the central plasma sheet on either side of midnight (51.7% pre-midnight, 48.3% post-midnight). IDRs identified using the method shown by A. J. Rogers et al. (2019) are also shown as an overlay of magenta circles on the TCS distribution in Figure 4. All of these IDRs are found in regions where MMS spent at least a moderate amount of time in a TCS. It should be noted that some IDR markers in Figure 4 and following figures totally obscure the dwell time indicator for the region where they are located. A listing of all IDRs plotted here is available in the supplementary materials.

Figure 4d shows the total TCS dwell time as a function of Magnetic Local Time (MLT). This subfigure is comparable with similar plots showing the global MLT distribution of other substorm-related phenomena such as Pi1B pulsations (Posch et al., 2007) and dipolarization fronts (Xiao et al., 2017), all of which show a strong preference for activity duskward of midnight.

Figure 5 shows the same TCS data derived from the parameter K_i but here normalized by the total dwell time MMS spent in the tail plasma sheet, as indicated by the measured ion number density $n_i > 0.05\ cc^{-1}$ (Baumjohann, 1993; A. J. Rogers et al., 2019). As expected, the majority of time spent by MMS in the tail plasma sheet was not near an ion-scale TCS, as indicated by the bulk of the distribution showing a ratio of TCS dwell time to plasma sheet

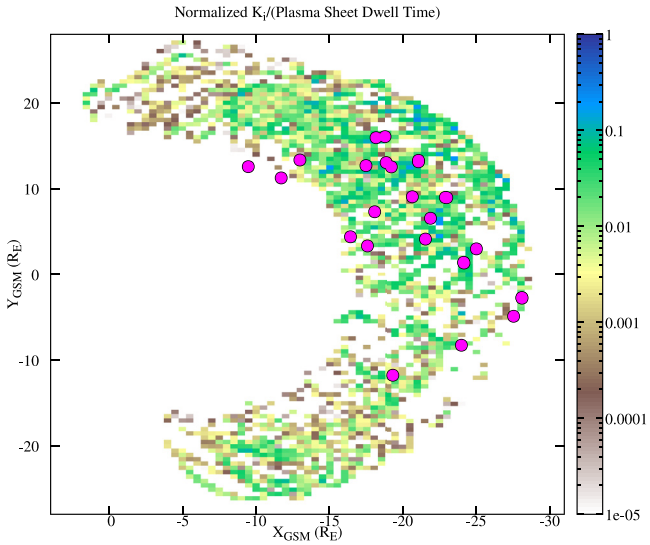

Figure 5. Dwell time MMS spent in a thin current sheet normalized by the amount of time MMS spent in the plasma sheet. Regions and projection are in the style of Figure 4a.

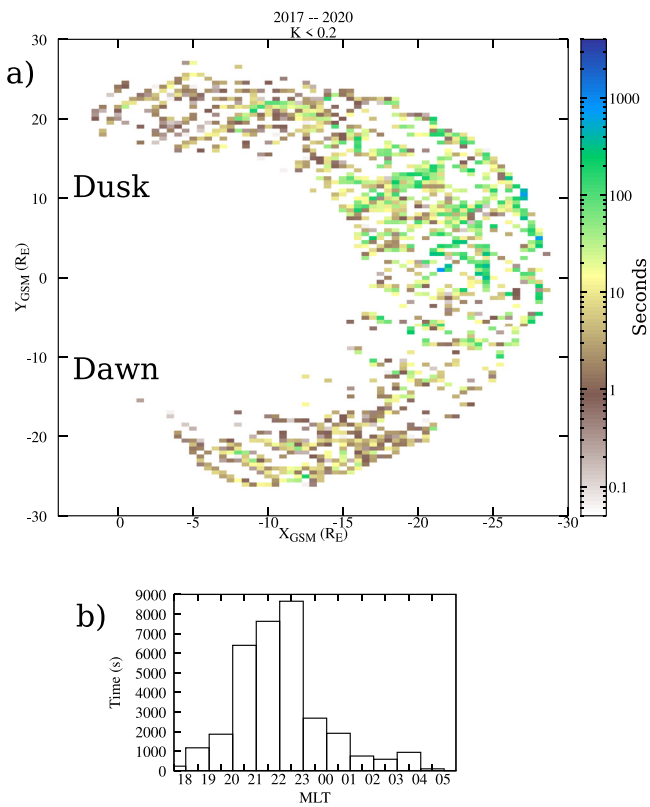

Figure 6. (a) Thin current sheet distribution where $K_i < 0.2$ in the style of Figure 4a. (b) The same distribution displayed as a function of MLT in the style of Figure 4d. While a more restrictive condition, the distribution does not qualitatively differ from that where $K_i < 1.0$.

dwell time of much less than one. The distribution of IDRs is again laid over the normalized dwell time map as it was in Figure 4.

The total time spent in a TCS is significantly higher on the pre-midnight side of the tail (187.8 hr) than the post-midnight (77.68 hr) as shown in Figure 4d. While MMS spent an approximately equal amount of time in the plasma sheet in both the pre- and post-midnight sectors (51.7%/48.3%), this contrasts with the *un*even amount of time spent in a TCS by MMS; 70.7% of total time in TCSs was in the pre-midnight sector versus 29.3% post-midnight; that is, far greater time was spent in a TCS on the duskside of midnight than the dawnside. The same calculations using the much more restrictive threshold of $K_i < 0.2$ (Büchner & Zelenyi, 1989) show qualitatively similar results with 78.9% of total TCS dwell time duskward of midnight and 21.1% dawnward of midnight and similar extent in radial distance (see Figure 6).

The majority of time spent in a TCS on the post-midnight side is found near apogee across all seasons (see Figure 4) where spacecraft velocity was the lowest and the bulk of dwell time was spent each orbit regardless of other factors. The distribution of time spent in a TCS pre-midnight is far more varied in radial distance and is not confined to the apogee of each orbit. Figure 7 shows the TCS dwell time of MMS as a function of MLT in bands of radial distance from the Earth, each $2R_E$ wide. The center of the relative TCS dwell time at smaller radial distances (Figures 7a and 7b) is substantially duskward of midnight at ∼21 MLT. The distribution broadens toward midnight as radial distance increases (Figures 7c and 7d), although the peak remains near 21MLT. Large relative TCS dwell times at the dawn and dusk flanks are interpreted as encounters with the flank magnetopause where CS and increased ion density are expected. Figure 7c represents the approximate region of the geomagnetic tail sampled by Cluster as in Rong et al. (2011).

The asymmetry in the locations of IDRs (magenta circles Figures 4 and 5) associated with magnetic reconnection is even more pronounced than that of relative TCS dwell time. Twenty one IDRs were confidently identified across all four tail seasons analyzed on the dusk-side of midnight, while only five were observed on the dawn-side, equating to 80.8% of reconnection event observed duskward of midnight and 19.2% dawnward. In Figure 5 we see that the majority of identified IDRs lie not only in areas where MMS spent a great deal of time in ion-scale TCSs, but also where the ratio of TCS dwell time to total plasma sheet dwell time was the greatest. This supports the intuitive interpretation that an ion-scale or thinner current sheet is more likely to support reconnection, and that reconnection is more likely where TCSs are more common.

4. Discussion

Such intuition was quantified by Y.-H. Liu et al. (2014) who used 2.5D PIC simulations to estimate that CS which thin to half-thicknesses of $\sim d_i$ will incur tearing instabilities, leading to reconnection. While the K_i parameter used in this study depends on the gyroradius of ions rather than inertial length, the requirement of $K_i < 0.2$ will provide an approximate comparison. However, there are long periods of time spent in both the plasma sheet and very TCS, as indicated by low K_i, where no reconnection was observed such as $-16R_E\hat{x}, 12R_E\hat{y}$ in Figure 6. This suggests that an ion-scale TCS alone is an insufficient condition for reconnection.

A feature of reconnection which stands out in observations is that IDRs and related phenomena occur preferentially in the pre-midnight sector (Eastwood

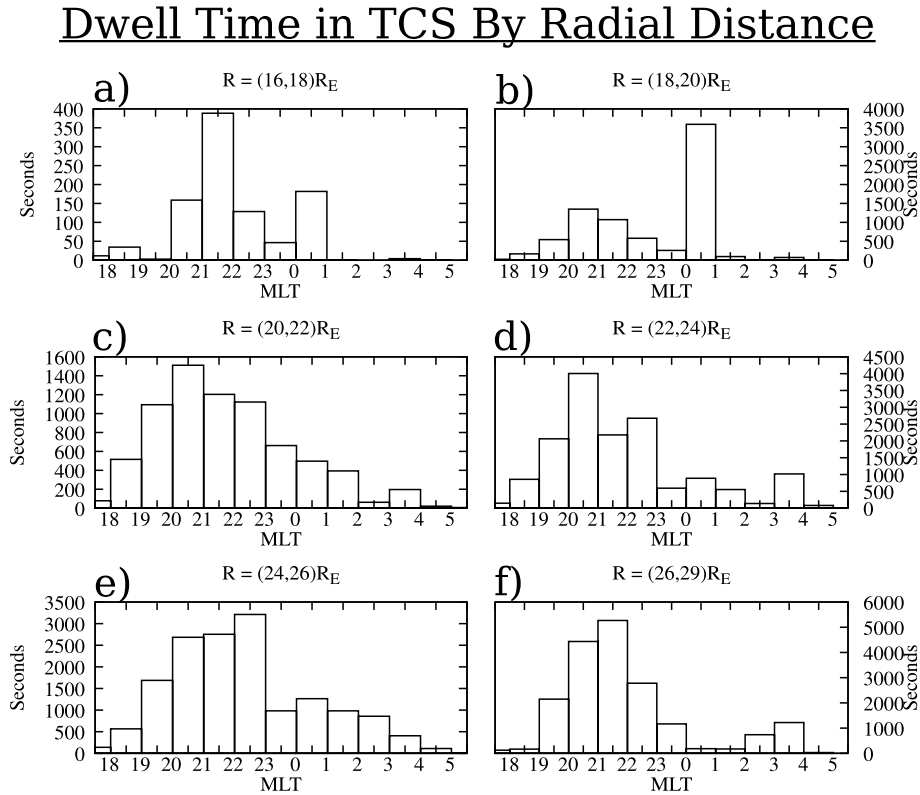

Figure 7. Dwell time MMS spent in a thin current sheet by MLT for narrow ($2R_E$ wide) bands across the geomagnetic tail. (c) Is the approximate region which has been studied by the Cluster mission (Rong et al., 2011).

et al., 2010; Genestreti et al., 2014; Nagai et al., 2013). The explanation for this has been glossed over somewhat since the question of observational bias due to orbital variations was not often addressed in a rigorous fashion (see discussion in Imber et al. (2011)). If an observatory spends more time near dusk then one supposes its chances of seeing IDRs or other phenomena is increased relative to other regions, all other things being equal. Thus while studies based on previous missions showed a dawn-dusk asymmetry in observed reconnection-related features, we as a field could not rule out an observational bias without rigorously including orbital statistics, something not commonly done in previous studies. This question was addressed by A. J. Rogers et al. (2019) who normalized observations by plasma sheet dwell time to strongly suggest that the asymmetric distribution of IDRs by MMS was not a function of observational bias, but is a result of magnetotail physics.

The seasonal dependence of substorms, wherein substorms occur more frequently near equinoxes than solstices (e.g., Russell & McPherron, 1973), combined with the direction of orbital precession, is another potential form of observational bias which may apply to the observations presented here. As MMS typically approached the duskside of the magnetotail nearer to the northern autumnal equinox and was typically on the dawnside nearer to the northern summer solstice, a greater number of substorms and dynamic changes to tail configuration during the later months might imitate a dawn-dusk asymmetry via seasonal variation in overall activity. However, studies of reconnection and related fast flow events made by Geotail near the northern winter solstice show a proportionally similar dawn-dusk asymmetry in event distributions as we have shown in TCS distribution (Nagai et al., 1998). Similarly, observations of ion heating in the near- to mid-tail by TWINS during CME and CIR related storms shows a strong duskward preference regardless of season (Keesee et al., 2014). And across the four tail seasons presented here, calculated K_i and the SuperMAG SML electrojet index (Gjerloev, 2012; Newell & Gjerloev, 2011) show no meaningful correlation ($r_{K,SML} = -0.02$). These observations strongly imply that whatever effect seasonal variations may have had on the results presented here, additional physics must be driving the observed asymmetry.

In addition to previous studies which observed a similar asymmetry but were more limited in extent (e.g., Rong et al., 2011) or utilized more indirect methods for calculating current sheet thickness (e.g., Lu et al., 2019),

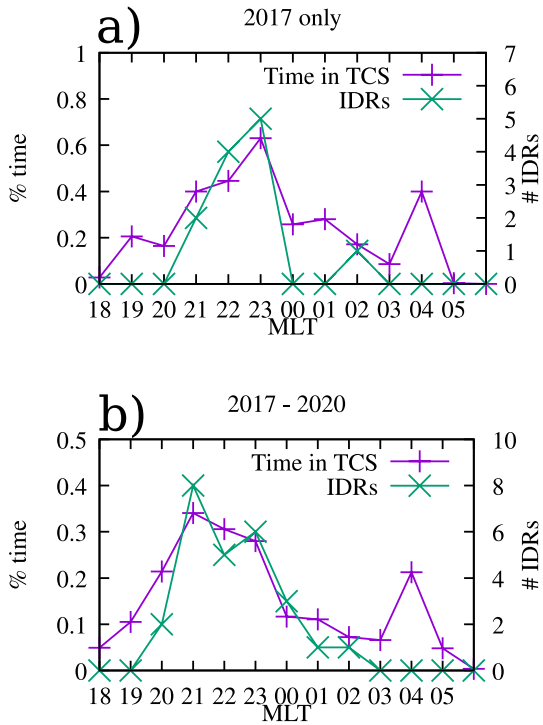

Figure 8. Plots of the proportion of the time MMS spent in a thin current sheet relative to total time spent in the plasma sheet as well as the location of identified IDRs, both as a function of MLT, for (a) the 2017 tail season and (b) the combined 2017–2020 tail seasons.

mechanisms for the source of this asymmetry have also been mooted. Lu et al. (2018) and Pritchett and Lu (2018) have hypothesized that the cause of this dusk-side preference was preferential thinning on the pre-midnight region of the tail due to an externally driven convective electric field and enhanced by Hall electric fields (normal to the central current sheet) which formed as the current sheet approached ion scales. Comparing our observations to this model we find the ratio of dwell time in an ion-scale TCS (70.7% pre-midnight to 29.3% post-midnight ≈2:1) qualitatively supports the model of Lu et al. (2018). A comparison of Figure 5 of the present work and Figure 2 in Lu et al. (2018) is even more encouraging as the radial variations in our observations are qualitatively similar to those shown in the PIC simulations.

We can also see the pre-/post-midnight TCS asymmetry clearly in Figure 8 which plots the time MMS spent in a TCS as a percentage of the total time spent in the plasma sheet. along with the number of IDRs identified in each MLT division. Simulations (Lu et al., 2016, 2018; Y. H. Liu et al., 2019; Pritchett & Lu, 2018) show that current sheet thinning precedes reconnection onset, generally followed by a rapid thickening. However, no effort has been made here to directly correlate any particular TCS encounter with a specific IDR encounter, or to determine conclusively that any or all TCSs encountered lead to reconnection. Regardless, it is unsurprising that the number of IDRs identified in a region of the magnetotail increases with the greater proportional time spent in a TCS. Less expected is the greater duskward extent of the TCS than of observed IDRs.

Recent 3D PIC simulations (Y. H. Liu et al., 2019) suggest that the near-midnight preference of observed reconnection may be due to the effects of Hall reconnection in three dimensions. Y. H. Liu et al. (2019) show that reconnection on a given TCS will be suppressed on the side of the current sheet opposite the direction of net electron flow for a region on the scale of 10 s of ion inertial lengths (see Figure 7 in Y. H. Liu et al. (2019)). In the geomagnetic tail, with a net dawnward current flow, this would lead to suppression of reconnection onset in the duskward side of an existing TCS. As shown above, ion-scale TCSs capable of supporting possible reconnection are twice as likely to be found on dusk-side of midnight as on the dawn-side. Thus while reconnection is more likely to occur pre-midnight in the tail due to ion-scale TCSs occurring more frequently there, it is more likely to be suppressed as the TCS extends further duskward away from midnight, see Figure 9 in Y. H. Liu et al. (2019). This would have the practical effect of concentrating reconnection onset in the region at and near midnight in the pre-midnight region. The location of nearly half of all identified IDRs is within the region of 22–24 MLT, supporting this hypothesis.

Also of note is the duskward expansion of both TCS and IDR locations over the four tail seasons analyzed here. 2017–2019 were in the declining phase of solar cycle 24, while the 2020 tail season was in the minimum between cycles, or the beginning of cycle 25. Figure 8a shows the distribution of proportional time in a TCS as well as IDR distribution in MLT for the 2017 tail season. The average daily sunspot number provided by OMNI data for 2017 was 21.8 when the duskward extent of TCSs observed by MMS extended much closer to the flank than the observed IDRs. Figure 8b shows the same distributions for the full four seasons studied here, during which time the daily sunspot number eased to an annual average of 3.6 in 2019 and averaged only 6.4 for the whole of 2018–2020. In the latter sub-figure the TCS and IDR distributions appear to be much more strongly correlated. This implies not only that the process of plasma sheet compression is a global process dependent on solar activity, consistent with the Dungey cycle (Dungey, 1963), but that the mesoscale process of asymmetric TCS distribution is also a function of solar driving, as suggested by simulation (Y.-H. Liu et al., 2014; Pritchett & Lu, 2018). More observations over the entire solar cycle are needed to properly investigate the influence of external drivers, such as local coupling to the solar wind convective electric field, on tail current sheet thickness.

5. Conclusion

In this work, we have shown a statistically significant Dawn–Dusk asymmetry in the distribution of TCSs in the geomagnetic tail across four MMS tail seasons. We have also shown a statistically significant concentration of Ion Diffusion Regions associated with magnetic reconnection in the pre-midnight sector. These observations have been compared to, and qualitatively support, recent hypotheses and simulations regarding the mechanisms governing such asymmetric distributions. Possible driving of these mechanisms, and through them the observed asymmetries, via increased solar activity is tantalizingly suggested, but continued observations throughout the solar cycle are necessary for any degree of certainty.

Data Availability Statement

All instrument data used in this study are publicly available at the MMS Science Data Center (https://lasp.colorado.edu/mms/sdc/public/). The OMNI sunspot data were obtained from the GSFC/SPDF OMNIWeb interface (https://omniweb.gsfc.nasa.gov).

Acknowledgments
The authors would like to thank Zach Dykstra and Phil Doroff for generous computational support, as well as Terry Forbes, Kevin Genestreti, and Matt Argall for many useful discussions. We gratefully acknowledge the SuperMAG collaborators (https://supermag.jhuapl.edu/info/?page=acknowledgement) for the SML index data. This work has been supported by NASA via contract 499878Q. LA-UR-23-20013.

References

Artemyev, A. V., Angelopoulos, V., Liu, J., & Runov, A. (2017). Electron currents supporting the near-Earth magnetotail during current sheet thinning. *Geophysical Research Letters*, *44*(1), 5–11. https://doi.org/10.1002/2016GL072011

Artemyev, A. V., Angelopoulos, V., & Runov, A. (2016). On the radial force balance in the quiet time magnetotail current sheet. *Journal of Geophysical Research: Space Physics*, *121*(5), 4017–4026. https://doi.org/10.1002/2016JA022480

Artemyev, A. V., Angelopoulos, V., Runov, A., & Petrokovich, A. A. (2016). Properties of current sheet thinning at $x \sim -10$ to -12 R_E. *Journal of Geophysical Research: Space Physics*, *121*(7), 6718–6731. https://doi.org/10.1002/2016JA022779

Artemyev, A. V., Petrukovich, A. A., Nakamura, R., & Zelenyi, L. M. (2011). Cluster statistics of thin current sheets in the Earth magnetotail: Specifics of the dawn flank, proton temperature profiles and electrostatic effects. *Journal of Geophysical Research*, *116*(A9), A09233. https://doi.org/10.1029/2011JA016801

Asano, Y., Nakamura, R., Baumjohann, W., Runov, A., Vörös, Z., Volwerk, M., et al. (2005). How typical are atypical current sheets? *Geophysical Research Letters*, *32*(3), L03108. https://doi.org/10.1029/2004GL021834

Baumjohann, W. (1993). The near-Earth plasma sheet: An AMPTE/IRM perspective. *Space Science Reviews*, *64*(1–2), 141–163. https://doi.org/10.1007/BF00819660

Birn, J. (1980). Computer studies of the dynamic evolution of the geomagnetic tail. *Journal of Geophysical Researc*h, *85*(A3), 1214–1222. https://doi.org/10.1029/JA085iA03p01214

Büchner, J., & Zelenyi, L. M. (1987). Chaotization of the electron motion as the cause of an internal magnetotail instability and substorm onset. *Journal of Geophysical Research*, *92*(A12), 13456–13466. https://doi.org/10.1029/ja092ia12p13456

Büchner, J., & Zelenyi, L. M. (1989). Regular and chaotic charged particle motion in magnetotaillike field reversals: 1. Basic theory of trapped motion. *Journal of Geophysical Research*, *94*(A9), 11821–11842. https://doi.org/10.1029/ja094ia09p11821

Cowley, S. W. H. (1981). Magnetospheric asymmetries associated with the y-component of the IMF. *Planetary and Space Science*, *29*(1), 79–96. https://doi.org/10.1016/0032-0633(81)90141-0

Dungey, J. W. (1961). Interplanetary magnetic field and the auroral zones. *Physical Review Letters*, *6*(2), 47–48. https://doi.org/10.1103/PhysRevLett.6.47

Dungey, J. W. (1963). Interactions of solar plasma with the geomagnetic field. *Planetary and Space Science*, *10*, 233–237. https://doi.org/10.1016/0032-0633(63)90020-5

Eastwood, J. P., Phan, T. D., Øieroset, M., & Shay, M. A. (2010). Average properties of the magnetic reconnection ion diffusion region in the Earth's magnetotail: The 2001-2005 Cluster observations and comparison with simulations. *Journal of Geophysical Research*, *115*(A8), A08215. https://doi.org/10.1029/2009JA014962

Fuselier, S. A., Lewis, W. S., Schiff, C., Ergun, R., Burch, J. L., Petrinec, S. M., & Trattner, K. J. (2016). Magnetospheric multiscale science mission profile and operations. *Space Science Reviews*, *199*(1–4), 77–103. https://doi.org/10.1007/s11214-014-0087-x

Genestreti, K. J., Fuselier, S. A., Goldstein, J., Nagai, T., & Eastwood, J. P. (2014). The location and rate of occurrence of near-Earth magnetotail reconnection as observed by Cluster and Geotail. *Journal of Atmospheric and Solar-Terrestrial Physics*, *121*, 98–109. https://doi.org/10.1016/j.jastp.2014.10.005

Gjerloev, J. W. (2012). The SuperMAG data processing technique: Technique. *Journal of Geophysical Research*, *117*(A9), A09213. https://doi.org/10.1029/2012JA017683

Harris, E. G. (1962). On a plasma sheath separating regions of oppositely directed magnetic field. *Il Nuovo Cimento* - B, *23*(1), 115–121. https://doi.org/10.1007/BF02733547

Henderson, M., Morley, S., Niehof, J., & Larsen, B. (2018). LANLGeoMag: V1.5.16 (version v1.5.16) [Dataset]. Zenodo. https://doi.org/10.5281/zenodo.1195041

Imber, S. M., Slavin, J. A., Auster, H. U., & Angelopoulos, V. (2011). A THEMIS survey of flux ropes and traveling compression regions: Location of the near-Earth reconnection site during solar minimum. *Journal of Geophysical Research*, *116*(A2), A02201. https://doi.org/10.1029/2010JA016026

Keesee, A., Elfritz, J., Fok, M.-C., McComas, D., & Scime, E. (2014). Superposed epoch analyses of ion temperatures during CME- and CIR/HSS-driven storms. *Journal of Atmospheric and Solar-Terrestrial Physics*, *115–116*, 67–78. https://doi.org/10.1016/j.jastp.2013.08.009

Liu, D., Lu, S., Lu, Q., Ding, W., & Wang, S. (2020). Spontaneous onset of collisionless magnetic reconnection on an electron scale. *The Astrophysical Journal*, *890*(2), L15. https://doi.org/10.3847/2041-8213/ab72fe

Liu, Y.-H., Birn, J., Daughton, W., Hesse, M., & Schindler, K. (2014). Onset of reconnection in the near magnetotail: PIC simulations. *Journal of Geophysical Research: Space Physics*, *119*(12), 9773–9789. https://doi.org/10.1002/2014JA020492

Liu, Y. H., Li, T. C., Hesse, M., Sun, W. J., Liu, J., Burch, J., et al. (2019). Three-dimensional magnetic reconnection with a spatially confined X-line extent: Implications for dipolarizing flux bundles and the dawn-dusk asymmetry. *Journal of Geophysical Research: Space Physics*, *124*(4), 2819–2830. https://doi.org/10.1029/2019JA026539

Lu, S., Artemyev, A. V., Angelopoulos, V., Lin, Y., Zhang, X. J., Liu, J., et al. (2019). The Hall electric field in Earth's magnetotail thin current sheet. *Journal of Geophysical Research: Space Physics*, *124*(2), 1052–1062. https://doi.org/10.1029/2018JA026202

Lu, S., Lin, Y., Angelopoulos, V., Artemyev, A. V., Pritchett, P. L., Lu, Q., & Wang, X. Y. (2016). Hall effect control of magnetotail dawn-dusk asymmetry: A three-dimensional global hybrid simulation. *Journal of Geophysical Research: Space Physics*, *121*(12), 11882–11895. https://doi.org/10.1002/2016JA023325

Lu, S., Pritchett, P. L., Angelopoulos, V., & Artemyev, A. V. (2018). Formation of dawn-dusk asymmetry in Earth's magnetotail thin current sheet: A three-dimensional particle-in-cell simulation. *Journal of Geophysical Research: Space Physics*, *123*(4), 2801–2814. https://doi.org/10.1002/2017JA025095

Morley, S. (2015). Magnetic Ephemeris and coordinates [Dataset]. Zenodo. https://doi.org/10.5281/zenodo.2594027

Nagai, T., Fujimoto, M., Saito, Y., Machida, S., Terasawa, T., Nakamura, R., et al. (1998). Structure and dynamics of magnetic reconnection for substorm onsets with Geotail observations. *Journal of Geophysical Research*, *103*(A3), 4419–4440. https://doi.org/10.1029/97JA02190

Nagai, T., Shinohara, I., Zenitani, S., Nakamura, R., Nakamura, T. K., Fujimoto, M., et al. (2013). Three-dimensional structure of magnetic reconnection in the magnetotail from Geotail observations. *Journal of Geophysical Research: Space Physics*, *118*(4), 1667–1678. https://doi.org/10.1002/jgra.50247

Nakamura, R., Baumjohann, W., Runov, A., Volwerk, M., Zhang, T. L., Klecker, B., et al. (2002). Fast flow during current sheet thinning: Fast flow during current sheet thinning. *Geophysical Research Letters*, *29*(23), 55-1–55-4. https://doi.org/10.1029/2002GL016200

Newell, P. T., & Gjerloev, J. W. (2011). Evaluation of SuperMAG auroral electrojet indices as indicators of substorms and auroral power. *Journal of Geophysical Research*, *116*(A12), A12211. https://doi.org/10.1029/2011JA016779

Petrukovich, A. A., Baumjohann, W., Nakamura, R., Runov, A., Balogh, A., & Rème, H. (2007). Thinning and stretching of the plasma sheet: Plasma sheet thinning and stretching. *Journal of Geophysical Research*, *112*(A10), A10213. https://doi.org/10.1029/2007JA012349

Pollock, C., Moore, T., Jacques, A., Burch, J., Gliese, U., Saito, Y., et al. (2016). Fast plasma investigation for magnetospheric multiscale. *Space Science Reviews*, *199*(1–4), 331–406. https://doi.org/10.1007/s11214-016-0245-4

Posch, J., Engebretson, M., Mende, S., Frey, H., Arnoldy, R., Lessard, M., et al. (2007). Statistical observations of spatial characteristics of Pi1B pulsations. *Journal of Atmospheric and Solar-Terrestrial Physics*, *69*(15), 1775–1796. https://doi.org/10.1016/j.jastp.2007.07.015

Pritchett, P. L., & Lu, S. (2018). Externally driven onset of localized magnetic reconnection and disruption in a magnetotail configuration. *Journal of Geophysical Research: Space Physics*, *123*(4), 2787–2800. https://doi.org/10.1002/2017JA025094

Raj, A., Phan, T., Lin, R. P., & Angeloppulos, V. (2002). Wind survey of high-speed bulk flows and field-aligned beams in the near-Earth plasma sheet. *Journal of Geophysical Research*, *107*(A12), SMP 3-1–SMP 3-17. https://doi.org/10.1029/2001JA007547

Rogers, A., & Rogers, T. (2022). Github.com/unh-mms-rogers/mms-curvature: MMS-curvature functioning beta [Dataset]. Zenodo. https://doi.org/10.5281/ZENODO.6456333

Rogers, A. J., Farrugia, C. J., & Torbert, R. B. (2019). Numerical algorithm for detecting ion diffusion regions in the geomagnetic tail with applications to MMS tail season 1 May to 30 September 2017. *Journal of Geophysical Research: Space Physics*, *124*(8), 6487–6503. https://doi.org/10.1029/2018JA026429

Rong, Z. J., Shen, C., Petrukovich, A., Wan, W., & Liu, Z. (2010). The analytic properties of the flapping current sheets in the Earth magnetotail. *Planetary and Space Science*, *58*(10), 1215–1229. https://doi.org/10.1016/j.pss.2010.04.016

Rong, Z. J., Wan, W. X., Shen, C., Li, X., Dunlop, M. W., Petrukovich, A. A., et al. (2011). Statistical survey on the magnetic structure in magnetotail current sheets. *Journal of Geophysical Research*, *116*(A9), A09218. https://doi.org/10.1029/2011JA016489

Runov, A., Angelopoulos, V., Artemyev, A., Weygand, J., Lu, S., Lin, Y., & Zhang, X.-J. (2021). Global and local processes of thin current sheet formation during substorm growth phase. *Journal of Atmospheric and Solar-Terrestrial Physics*, *220*, 105671. https://doi.org/10.1016/j.jastp.2021.105671

Runov, A., Sergeev, V. A., Baumjohann, W., Nakamura, R., Apatenkov, S., Asano, Y., et al. (2005). Electric current and magnetic field geometry in flapping magnetotail current sheets. *Annals of Geophysics*, *23*(4), 1391–1403. https://doi.org/10.5194/angeo-23-1391-2005

Runov, A., Sergeev, V., Nakamura, R., Baumjohann, W., Zhang, T., Asano, Y., et al. (2005). Reconstruction of the magnetotail current sheet structure using multi-point Cluster measurements. *Planetary and Space Science*, *53*(1–3), 237–243. https://doi.org/10.1016/j.pss.2004.09.049

Russell, C. T., Anderson, B. J., Baumjohann, W., Bromund, K. R., Dearborn, D., Fischer, D., et al. (2016). The magnetospheric multiscale magnetometers. *Space Science Reviews*, *199*(1–4), 189–256. https://doi.org/10.1007/s11214-014-0057-3

Russell, C. T., & McPherron, R. L. (1973). Semiannual variation of geomagnetic activity. *Journal of Geophysical Research*, *78*(1), 92–108. https://doi.org/10.1029/JA078i001p00092

Sergeev, V., Angelopoulos, V., Carlson, C., & Sutcliffe, P. (1998). Current sheet measurements within a flapping plasma sheet. *Journal of Geophysical Research*, *103*(A5), 9177–9187. https://doi.org/10.1029/97JA02093

Shen, C., Rong, Z. J., Li, X., Dunlop, M., Liu, Z. X., Malova, H. V., et al. (2008). Magnetic configurations of the tilted current sheets in magnetotail. *Annales Geophysicae*, *26*(11), 3525–3543. https://doi.org/10.5194/angeo-26-3525-2008

Sibeck, D. G., & Angelopoulos, V. (2008). THEMIS science objectives and mission phases. *Space Science Reviews*, *141*(1–4), 35–59. https://doi.org/10.1007/s11214-008-9393-5

Sitnov, M., Birn, J., Ferdousi, B., Gordeev, E., Khotyaintsev, Y., Merkin, V., et al. (2019). Explosive magnetotail activity. *Space Science Reviews*, *215*(4), 31. https://doi.org/10.1007/s11214-019-0599-5

Torbert, R. B., Russell, C. T., Magnes, W., Ergun, R. E., Lindqvist, P.-A., LeContel, O., et al. (2016). The FIELDS instrument suite on MMS: Scientific objectives, measurements, and data products. *Space Science Reviews*, *199*(1–4), 105–135. https://doi.org/10.1007/s11214-014-0109-8

Xiao, S., Zhang, T., Wang, G., Volwerk, M., Ge, Y., Schmid, D., et al. (2017). Occurrence rate of dipolarization fronts in the plasma sheet: Cluster observations. *Annals of Geophysics*, *35*(4), 1015–1022. https://doi.org/10.5194/angeo-35-1015-2017